Journal of Molecular Liquids 306 (2020) 112895

Contents lists available at ScienceDirect

Journal of Molecular Liquids

journal homepage: www.elsevier.com/locate/molliq

Co-electrospun polysuccinimide/poly(vinyl alcohol) composite meshes for tissue engineering

Constantinos Voniatis [a,b], Lukas Balsevicius [a], Dóra Barczikai [a], David Juriga [a], Angéla Takács [c], László Kőhidai [c], Krisztina Nagy [a], Angela Jedlovszky-Hajdu [a,*]

[a] Laboratory of Nanochemistry, Department of Biophysics and Radiation Biology, Semmelweis University, Budapest, Hungary
[b] Department of Surgical Research and Techniques, Semmelweis University, Budapest, Hungary
[c] Department of Genetics, Cell- and Immunobiology, Semmelweis University, Budapest, Hungary

ARTICLE INFO

Article history:
Received 3 February 2020
Received in revised form 9 March 2020
Accepted 12 March 2020
Available online 17 March 2020

Keywords:
Electrospinning
Fibrous composite mesh
PSI/PVA fibres
Mechanical study
Cell viability

ABSTRACT

One of the most focused-on point in biomedical and biotechnological research is the fabrication of complex tissue engineering scaffolds, with the ultimate objective being a functional, biocompatible and biodegradable implant that could facilitate and enhance tissue regeneration. Creating such implants is a highly challenging task. Physical and chemical characteristics have to be optimized and the balance between biodegradability, mechanical strength and overall practicality cannot be easily obtained. In this regard, composite materials have been regularly used in numerous areas of science and engineering as they incorporate advantages from two or more component materials. Our objective was to fabricate a composite, fibrous mesh composed of both degradable and non-degradable elements, that could be applicable as an implant with reliable mechanical properties without hindering in vivo tissue integration. In the manuscript, we present the fabrication, chemical, physical, mechanical and cytotoxic evaluation of co-electrospun polysuccinimide/poly(vinyl alcohol) (PSI/PVA) meshes. Results confirmed the presence and random distribution of both PSI and PVA fibres in the fabricated meshes. Mechanical studies indicate that meshes are competent for implantation while cell viability study revealed no cytotoxic effects.

1. Introduction

Tissue engineering is a multidisciplinary field aiming to regenerate damaged or replace lost tissues. The three main approaches to tissue engineering include a. Chemical techniques using drugs and signalling molecules to induce a direct, in vivo cellular proliferation and differentiation thus slowly developing new tissues [1] b. Biological methods, where ex vivo cell cultures are established utilizing cells extracted from the patient herself/himself or a donor which will be subsequently implanted back to the patient [2] and c. Physical systems namely biomaterials and tissue scaffolds which are directly implanted serving as a framework where the innate cells of the patient can adhere, proliferate and differentiate [3]. Furthermore, hybrid methods i.e. combinations of two or more of the above methods have been examined as well [4]. Tissue scaffolds can be fabricated using either natural/biological or synthetic materials with each one having its own advantages and disadvantages. Polymers, are very prominent materials for scaffold fabrication. Their synthesis is feasible with several methods (e.g. via thermal polycondensation, ring-opening polymerization, enzymatic polymerization), they have numerous possibilities for modifications (e.g. via curing, grafting, derivatization) and most of them have effective manufacturing methods (e.g. solution polycondensation, melt polycondensation) making polymers the most frequently used materials for the design and production of biomaterials [5].

Polymer-based biomaterials are already widely used in medicine: from dental implants to vascular grafts to abdominal wall prostheses [6,7]. However, one of the current aims of tissue engineering is to fabricate biomaterials that will be degraded (after fulfilling their purpose) and disappear while the patient's own cells proliferate and differentiate, regenerating the lost tissue by having used the implant as a framework [8]. Unfortunately, the application of fully biodegradable biomaterials is limited as finding the perfect balance between the mechanical strength, the duration of biodegradability, the desired functionality yet manageable costs is a huge challenge [9].

Apart from its chemical and physical composition, a biomaterial's microstructure has a huge impact on the implant-host tissue interaction. Logically, an implant should resemble and match the structure and characteristics of the original tissue. Accordingly, one widely accepted tactic, especially for soft tissue implants, is to produce fibrous

* Corresponding author at: Nagyvárad square 4, 1089 Budapest, Hungary.
E-mail address: hajdu.angela@med.semmelweis-univ.hu (A. Jedlovszky-Hajdu).

https://doi.org/10.1016/j.molliq.2020.112895

biomaterials aiming to mimic the extracellular matrix, a component found in almost every tissue surrounding cells providing physical and biochemical support [10].

Electrospinning is a commonly used technique to fabricate polymer meshes composed of micro- or even nano-sized fibres. The simplest form of the technique involves transferring a polymer solution to a syringe with an attached needle which is connected to a high-power voltage supply. As the solution is slowly pushed through by an infusion pump, the polymer droplet at the end of the needle will elongate as the electric force increases, overcoming the surface tension of the polymer solution. Droplets are then expelled, fly towards and finally adhere onto a grounded collector while simultaneously the polymer-solvent evaporates resulting in the formation of polymer fibres. While electrospinning is perhaps the simplest and most cost-effective technique to fabricate tissue scaffolds, it is quite versatile and can be easily modified resulting in enhanced, complex, functionalized meshes [11,12].

Poly(vinyl alcohol) (PVA) is a well-known, water-soluble, biocompatible polymer that has already been utilized for biomedical applications mostly in colloidal (e.g. eye drops) and hydrogel forms (e.g. contact lenses, cartilage grafts) [13]. Electrospun PVA meshes have been examined before as potential tissue scaffolds demonstrating a non-toxic, minimally immune reactive, biocompatible nature [14]. Nevertheless, some difficulties have been observed regarding cell adhesion, infiltration and tissue integration [14,15]. These are issues commonly observed when examining potential biomaterials or tissue scaffolds and several approaches have been examined as potential solutions to the problem (use of anti-inflammatory drugs, corticosteroids, biologically active molecules etc.) [16].

Conversely, poly(succinimide) (PSI) is a relatively recently developed polymer which has been investigated as a drug delivery system and biodegradable tissue scaffold [17,18]. While its biocompatibility is highly suggested [18,19], its mechanical performance and short degradation time [20] limit the spectrum of its application possibilities. The two polymers having individual advantages and disadvantages of their own could be combined to form a composite material which perhaps could demonstrate synergistic properties.

PVA has been proven to have excellent mechanical properties, even being a suitable material for surgical hernia mesh [14]. Furthermore, the water solubility of PVA makes the addition of active pharmaceutical ingredients (antibiotics, analgesics, anti-inflammatory drugs) a simple matter, something researchers have exploited numerous times [21,22]. On the contrary, PSI is a water-insoluble polymer that is susceptible to enzymatic degradation under physiological conditions [23]. Apart from its biocompatible nature, PSI is a polymer that can be easily functionalized due to the monomer's imide group which have been proven to react with nucleophilic molecules even under mild conditions [18,24].

Co-electrospinning is a branch technique where two individual polymer solutions are electrospun at the same moment resulting in a composite material composed of two different polymer fibres [25]. Although seemingly a simple modification the resulting composite mesh may have enhanced physical, chemical or mechanical characteristics. The objective of this work was to attempt combining PSI and PVA fabricating a composite co-electrospun nanofibrous mesh. Our primary aim was to fabricate a composite tissue scaffold with a degradable and non-degradable component to enhance cell adhesion, infiltration and overall tissue integration while still providing a stable foundation for the cells and retaining its mechanical strength. Additionally, in the future, both polymer fibres could also be utilized to encapsulate drugs resulting in a complex drug delivery system where two synergistically acting drugs can be delivered together or even a system which is able to deliver water-soluble and -water insoluble drugs concurrently [26].

In this work, we present the fabrication of co-electrospun composite PSI/PVA meshes, their physical and chemical characterization with scanning electron microscope (SEM), two-photon excitation microscopy (TPEM), and infrared spectroscopy (ATR-FTIR), their mechanical characterization and finally an examination of in vivo cell-mesh reactions with two different cell lines (A2058 melanoma and MeWo malignant melanoma cell line).

2. Materials and methods

2.1. List of materials

Poly(Vinyl Alcohol) (Mowiol® 10–98, Mw ~61,000, Sigma Aldrich, USA), Glutaraldehyde (25%, Merck, Germany), Hydrochloric Acid (37%, Reanal Labor), Chlorine Dioxide (3350 Ppm, Solvocid, Hungary), L-Aspartic Acid (Reagent Grade ≥ 98%, Mw ~133, Sigma Aldrich, USA), Orthophosphoric Acid (Reagent Grade ≥ 99%, Mw ~98, Sigma Aldrich, USA), Dimethylformamide (Anhydrous, Reagent Grade 99.9%, VWR International), Nile Blue A Stain (Dye Content ≥75%, Sigma Aldrich, USA), Ultrapure Water (Water Purification System, Zaneer), Phosphate-Buffered Saline (Sigma Aldrich, USA), Sodium-azid (Sigma Aldrich, USA), RPMI 1640 Medium (Sigma-Aldrich, USA), Fetal Bovine Serum (FBS) (Gibco, USA), L-Glutamine (Lonza, Switzerland), Penicillin-Streptomycin (Gibco, USA), Eagle's Minimum Essential Medium (Lonza Bioscience, Switzerland), Dulbecco's Modified Eagle Medium (Lonza Bioscience, Switzerland), Non-Essential Amino Acid (NEAA) Solution (Gibco, USA), Trypsin (Gibco, USA), Paraformaldehyde (4% Sigma Aldrich, USA), Vybrant™ DiD Cell-Labeling Solution (Thermo Fisher Scientific), alamarBlue™ Cell Viability Reagent (Thermo Fisher Scientific, USA).

2.2. Synthesis of polysuccinimide

Polysuccinimide (PSI) is the product of the thermal polycondensation of L-aspartic in the presence of phosphoric acid. L-aspartic acid and phosphoric acid were mixed at a 1:1 ratio and subsequently sealed in a flask. The flask was connected to a rotary vacuum evaporator system with a silicon oil bath (RV10 digital rotary evaporator, IKA, Germany). The mixture was gradually heated up to 180 °C while the pressure inside the flask was gradually decreased to 5 mbar. The mixture was left to rotate at a constant speed for 8 h. Further details about the synthesis and information about the quality control (polymerization yield, average molar mass and molar mass distribution) can be found in the research group's previous publication [27], where the molar mass was calculated by the Kuhn-Mark-Houwink equation following viscosity measurements according to the methodology of J. Vlasak et al. [28].

2.3. Preparation of the polymer solutions

PSI was dissolved in dimethylformamide(DMF) to gain a 25 *w*/w % concentration solution. To produce the PVA solution, PVA pellets were added to heated (90 °C) and vigorously stirred water. The solution was stirred until the pellets fully dissolved and a homogenous solution was observed. The polymer solution was then left to cool down to room temperature. The concentration of the raw unprocessed solution was determined by gravimetric analysis. The exact concentration used for the electrospinning (18 *w*/w %) was then adjusted by the addition of water if required. Stock solutions of PVA and PSI were kept in refrigeration until used. Exactly before electrospinning 327 μl of 1 M glutaraldehyde (GDA) solution was thoroughly mixed to 4 ml of PVA solution. GDA was used as a cross-linking agent with cross-link density of 50, (i.e. every 50th monomer is theoretically crosslinked) for both the pure PVA and PSI/PVA meshes [14].

2.4. Electrospinning setup

To fabricate the single polymer meshes, the standard electrospinning setup was used. Polymer solutions were transferred to 5 ml Luer-slip syringes (Chirana, Slovakia) with customized 18G needles (Becton Dickinson, USA). Polymer solutions were delivered by an infusion pump

(KDS100, KD Scientific, USA) at a constant flow rate. The desired electric potential was provided by a high voltage DC supply (73030P series, Genvolt, UK) the positive electrode was clamped on the needle while the ground electrode was attached to the rotating collector (RPM = 50). For the composite meshes, a co-electrospinning setup was designed to electrospin the two polymer solutions simultaneously at a 1:1 mass ratio (Fig. 1.). Electrospinning parameters can be found in Table 1.

2.5. Post-electrospinning processing

After extraction from the collector, meshes underwent physical and chemical treatments. All types of meshes (PSI, PVA, PSI/PVA) were folded into 10 × 10 cm squares. After the folding, meshes were compressed with 5 t of pressure along their entire surface for 5 min with an RH-97331 Hydraulic Press (Shanghai Reach Automotive, China). In the case of the PVA and PSI/PVA meshes, immersion in 2 M HCl for 1 h was essential in order for the cross-linkage formation to occur [14]. After the chemical treatment samples were extensively washed with ultrapure water until the pH reached a value of 7. PSI samples were stored dry, at room temperature while PVA and PSI/PVA samples were stored in sterilized ultrapure water at 4 °C.

2.6. Attenuated total reflectance Fourier transform infrared (ATR-FTIR) spectroscopy

Chemical analysis of the samples was performed using a FT/IR spectrophotometer (4700 series type A, JASCO, Japan), equipped with a diamond ATR head (ATR Pro One, JASCO, Japan). All measurements were carried out in a mid-infrared range of wavelength (4000–400 cm^{-1}), with 2 cm^{-1} resolution and 126 total number of scans. Before sample analysis, background spectra (H_2O, CO_2 subtraction) were obtained on a clean and dry diamond crystal and were subtracted from the sample spectra. PSI samples were examined dry, directly after the electrospinning. PVA and PSI/PVA samples were examined before (dry state) and after the chemical treatment (after washing and drying). Additionally, PSI/PVA samples were also examined after 1st, 3rd and 5th days of incubation in a sterile, room temperature PBS solution (after being washed and dried).

2.7. Scanning electron microscopy

To verify the fibrous microstructure, measure the thickness and assess the size distribution of the fibres, scanning electron microscopy was utilized. Small samples (25 mm^2) were cut from all the preprocessed samples. Due to absorbing liquid, chemically treated samples namely PVA and PSI/PVA required lyophilization before their examination. Images were taken with a JSM 6380LA scanning electron microscope (JEOL, Japan). After securing them on an adaptor with conductive stickers, samples were subsequently coated with a thin layer of gold using a JFC-1200 Sputter Coating System (JEOL, Japan). The applied voltage was 15 kV and micrographs were obtained at a 1000×, 5000× and 10,000× magnifications. Average fibre diameter and size distribution were determined by measuring 100 individual fibres. Measurements were performed using Fiji software (Open Source Software).

2.8. Two-photon excitation microscopy

Additionally, in the case of the composite meshes (PSI/PVA) to examine and visualize the presence and distribution of the two polymers two-photon excitation microscopy was utilized. PSI fibres can be observed as produced without staining, due to their auto-fluorescent nature [29,30]. PVA fibres were stained with Nile Blue A stain (0.5 wt% of PVA). A Femto2D series (Femtonics, Hungary) two-photon microscope was used. Photo-activity of samples was induced with a DeepSee™ laser (Spectra Physics, United States), at a wavelength of 800 nm. Images were taken with a 10× and 60× objectives.

2.9. Contact angle measurements

Assessment of wettability was possible by measuring the water contact angle on the different meshes. Small circular samples (d = 1.5 cm) were prepared from the electrospun fibrous meshes. For the measurement, PVA and PSI/PVA samples were extensively dried. Distilled water was transferred to a 50 μl Hamilton syringe with a 0.56 mm needle then, a droplet (5 μl) was carefully placed on the centre of the samples Investigations were performed using a contact angle meter with a built-in camera (OCA 15 Plus, Dataphysics, Germany).

2.10. Mechanical studies

Evaluation of mechanical parameters is essential for any type of tissue engineering implant. For the mechanical studies, rectangle samples (2 cm × 6 cm) were prepared from every mesh. Samples of both horizontal ($n = 5$) and vertical (n = 5) direction to the direction of the rotating collector were measured. For the assessments, a uniaxial mechanical tester (4952, Instron, USA) was utilized. Samples were assessed before and after the mechanical and chemical treatment. Untreated samples were measured in air (Temperature: 25 °C, Humidity: 28%) while treated samples were measured under physiological saline solution (0.9 *w*/w %, 25 °C) at a 1 mm/min pulling speed.

2.11. Cell studies

Cell viability studies were performed to examine any possible cytotoxic effects from the meshes. Two types of human tumour cell lines: A2058 melanoma cell line (ATCC CRL-11147) and MeWo malignant melanoma cell line (ATCC HTB-65) were cultured as subconfluent monolayers under standard conditions (100% humidity, 37 °C and 5% CO_2). The A2058 cells were cultured in RPMI 1640 medium (Sigma-

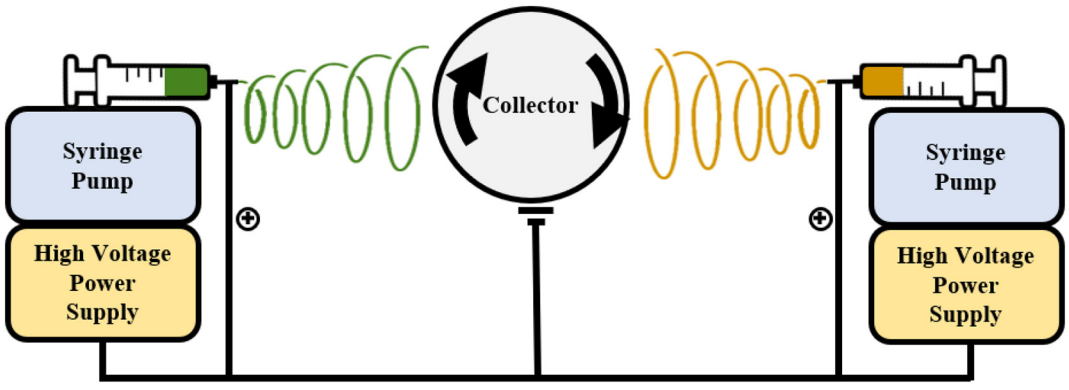

Fig. 1. Co-electrospinning setup.

Table 1
The applied parameters for the single and co-electrospinning.

Mesh type	Polymer concentration	Flow rate (ml/h)	Voltage (kV)	Collector distance (cm)
Single polymer mesh - PSI	(25 w/w%)	1	13.5	15
Single polymer mesh - PVA	(18 w/w%)	0.7	18	15
PSI/PVA composite polymer mesh	(25/18 w/w%)	0.5/0.7	13.5/18	15

Aldrich, USA) supplemented with 10% foetal bovine serum (FBS) (Gibco, USA), 2 mM L-glutamine (Lonza, Switzerland), 100 units/ml penicillin and 100 mg/ml streptomycin (Gibco, USA). The growth medium for MeWo cells consisted of Eagle's Minimum Essential Medium containing 10% FBS (Gibco, USA), 1% non-essential amino acids (Gibco, USA), 2 mM L-glutamine (Lonza, Switzerland), 100 units/ml penicillin and 100 mg/ml streptomycin (Gibco, USA). Disks with a diameter of 6 mm were cut from each mesh. Before adding the polymer meshes to the cells, they were sterilized in 0.1% chlorine-dioxide solution (in PBS) for 10 min. In case of both melanoma types, 10 000 cells/well were seeded into 96 well microplates in 200 μl culture medium/well and incubated at 37 °C for 24 h. Afterwards, the culture medium was replaced by 200 μl fresh medium/well and a single disk was placed into each well. Cell viability was evaluated by a colorimetric assay 24 and 48 h after the treatments with the meshes. Firstly, the polymer meshes were removed from the cell culture medium, then 22–22 μl of the alamarBlue® Cell Viability Reagent (10×) solution (Thermo Fisher Scientific, USA) was added to each well. After a 3-h incubation with the alamarBlue® reagent, the fluorescence intensity was measured by means of a LS-50B Luminescence Spectrometer (Perkin Elmer, UK) applying 560 nm as an excitation wavelength and 590 nm for detection of the emitted light.

3. Results and discussion

3.1. Co-electrospinning

No issues were observed with either polymer during the co-electrospinning. The single polymer meshes and the composite PSI/PVA mesh are macroscopically identical and there seems to be a difference only in texture as the composite meshes are fleecier.

3.2. Post-electrospinning processing

One of the most prominent disadvantages of single needle electrospinning is the slow production rate (e.g. 0.5–1.5 ml of polymer solution per hour) resulting in thin and fragile meshes. Various methods have been developed for increasing production rates (e.g. multiple spinnerets, needleless electrospinning) [11]. In our case, a more practical approach was chosen to reinforce and enhance the mechanical characteristics of the meshes, therefore, increasing the overall resistance to handling during in vitro cell studies or ensuing in vivo animal experiments. After the mechanical treatment (folding and compression), meshes became compact and rigid. Furthermore, PVA being a water-soluble material requires some type of cross-linkage to prevent the instant dissolution of the meshes at physiological environmental conditions. After the chemical treatment and extensive washing, PVA meshes become opaque and gelatinous. This change is due to the cross-linking reaction as the polymer fibres absorb surrounding liquid and become gel fibres. [14,31,32]. On the contrary, PSI/PVA composite meshes are still matte white but become soft and flexible (Fig. 2).

3.3. Chemical characterization

The obtained FTIR spectra for the electrospun meshes are shown in Fig. 2. The peaks obtained from the PSI samples are in accordance with the peaks in previous works of our own [24,33] and other research groups [18] as well. Specifically, the peak at 3596 cm^{-1} marks the O—H groups, the one at 2961 cm^{-1} the C—H bonds [34]. The peak at 1709 cm^{-1} corresponds to the imide rings (asymmetric stretching vibration) while the peak at 1380 cm^{-1} for the C—O (bending vibration) [27]. Examining the spectra of the PVA samples we can clearly see how the O—H peak at 3303 cm^{-1} decreases after the chemical treatment as the GDA crosslinking takes place. Additionally, peaks at 2905 cm^{-1}, 1418 cm^{-11} and 1076 cm^{-1} mark the C—H, C—O and C-O-C bonds respectively and remain unaffected [35]. As expected, the spectra of the composite mesh demonstrate characteristic peaks of both polymers but also the decrease of the O—H group after the chemical treatment due to the cross-linkage formation (Fig. 3). Examining the PSI/PVA samples incubated in PBS, no detectable change was observable after 24 h but the 3rd and 5th day samples show a slight decrease of some of the O—H peak (see Supplementary Fig. 1).

3.4. Physical characterization

3.4.1. Scanning electron microscopy

The images obtained with the scanning electron microscope display that throughout the entire fabrication process all the produced meshes retain their nanofibrous microstructure unaffected from the mechanical (compressing) and chemical (cross-linking) processing (Fig. 4).

While initially, the PSI meshes have thicker fibres than the PVA meshes, after the chemical treatment fibres absorb liquid (gel-fibre formation) and become thicker with a final average diameter close to the PSI samples. Furthermore, while retaining the overall microstructure, PVA fibres positioned too close to each other can adhere then fuse, forming larger fibres which we regarded as a single fibre that may

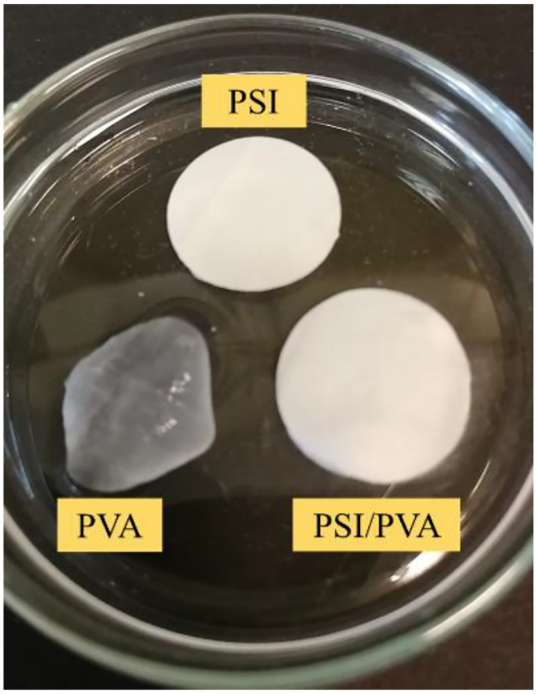

Fig. 2. PSI, PVA(post-treatment) and PSI/PVA (post-treatment samples in PBS.

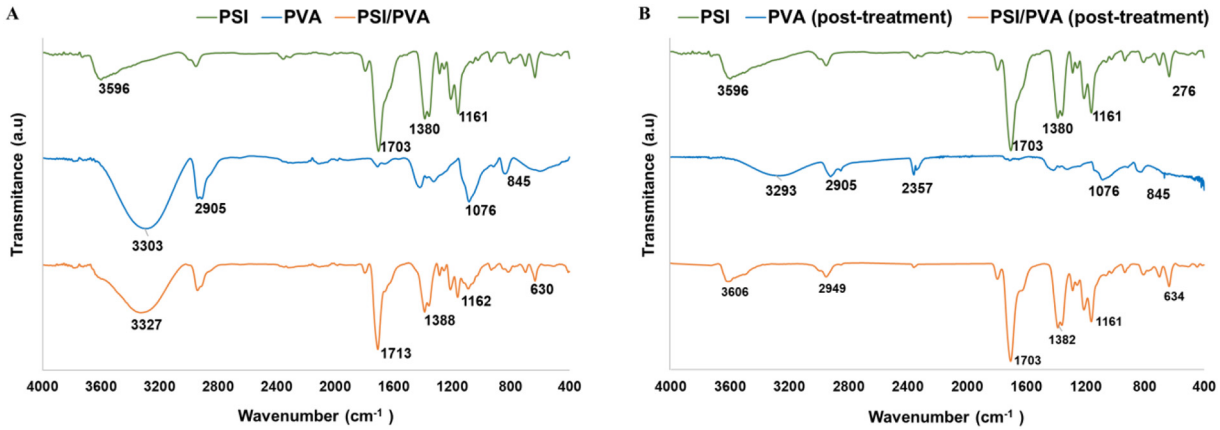

Fig. 3. ATR-FTIR spectra of electrospun meshes before (A) and after (B) the chemical treatment.

explain discordance of the average diameter in some cases [24]. The average fibre diameter of the examined meshes can be found in Table 2.

Observing the histogram (Fig. 5) of the composite PSI/PVA meshes we can see two peaks compared to the normal Gaussian distribution obtained from the single polymer meshes (see Supplementary Figs. 2 and 3) further confirming the presence of two types of fibres in one mesh. Furthermore, the peaks move after the post-electrospinning processing as the PVA fibres become thicker.

3.4.2. Two-photon excitation microscopy

Two-photon microscopy proved to be an effective method to visualize the spatial distribution of the fibres over the composite PSI/PVA meshes. PSI has the ability to highly fluoresce at around 600 nm wavelength without requiring staining (autofluorescence was previously published by Juriga et al. [33]). In order to distinguish the PSI and PVA fibres, Nile Blue dye was utilized to stain the PVA fibres red at the same time as PSI fibres would emit green light. Micrographs show that both fibres types are randomly distributed across the entire sample (Fig. 6). In addition, a *Z*-stack of the PSI/PVA samples was also prepared (see Supplementary Materials).

3.4.3. Wettability

In general terms, wettability defines the bonding ability of different materials resulting from the intermolecular forces in question [36]. Regarding tissue engineering, measuring the water contact angle of tissue scaffolds is essential as wettability highly influences cell adhesion and therefore tissue integration [37,38]. In addition, to our knowledge wettability of electrospun PSI had yet to be performed. Water angle measurement was not successful with all the meshes (Table 3). In the case of the PVA meshes a contact angle of 44.7° was measured, then additional measurements were repeated with wet PVA samples measuring an angle of 66.4° (Fig. 7). Based on the literature [39] it is obvious that the dried PVA mesh showed more hydrophilicity than the already wetted one. The wet PVA mesh already contains water, the fibres are already in a swelled state, thus less water can penetrate to the mesh, which results in the increase of the water contact angle [26]. Measuring a water contact angle for the PSI and PSI/PVA composite was not possible due to fast droplet disappearance. In the case of the PSI, the droplet instantaneously penetrates the sample. The PSI itself is hydrophobic, but the fibrous structure has a capillary effect due to the surface roughness, thus instead of retaining the droplet on the mesh surface, the droplet is

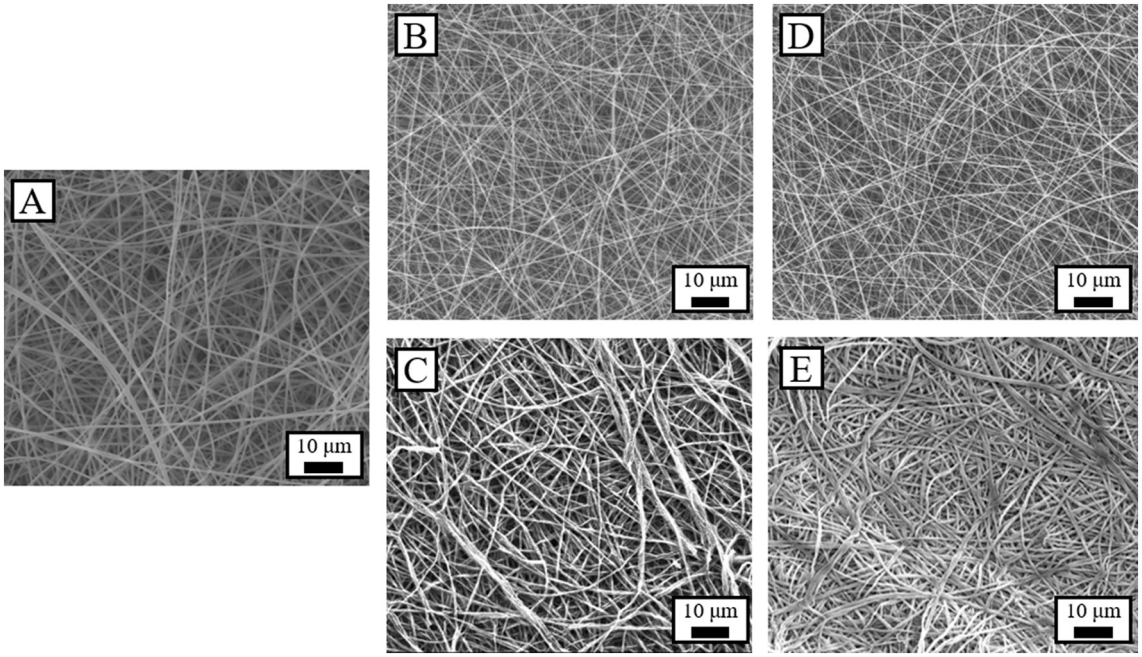

Fig. 4. SEM micrographs of electrospun meshes: PSI (A), PVA before (B) and after (C)treatment, PSI/PVA before(D) and after (E) treatments.

Table 2
The average fibre diameter of fabricated samples.

Mesh type	Average fibre diameter (nm)
PSI	614 ± 106
PVA	267 ± 59
PVA (post-treatment)	598 ± 139
PSI/PVA composite	359 ± 69
PSI/PVA composite (post-treatment)	789 ± 103

drawn in, a phenomenon already described in current literature [40]. The PSI/PVA sample exhibited a similar behaviour but as the droplet passed through the samples starts to swell as the PVA fibres absorb it. The droplet took a slightly longer time to pass through the sample. As the droplet passed though, the sample started to swell due to absorbing the water. Both attempts can be seen on video (see Supplementary Materials).

3.5. Mechanical characterization

The setup of the mechanical measurements can be found in Fig. 8. A comprehensive mechanical study is essential for any type of tissue engineering implant. In our case, we examined the meshes before and after the treatments and in both orientations of the rotating collector in order to gain as much information as possible regarding the strength of the meshes. All samples exhibited a similar behaviour (Fig. 8, E) as described in our and other works with evaluation of mechanical parameters of electrospun membranes [14,41,42]. Stress-strain curves for the single polymers meshes can be found in the supplementary information (see Supplementary Fig. 4).

The produced meshes were so thin that measuring their thickness with a calliper proved unreliable resulting in extraordinary loading capacities when calculated by force per thickness (N/cm) or force per surface (N/cm^2). To make the evaluation as objective as possible results were calculated in force (N) per area density or in other words grammage (g/m^2). Results can be found in Table 4. Between the untreated samples, PVA is slightly stronger than the PSI. As the mass and size of the samples are normalized the cause of this difference is probably the difference in fibre diameter (Table 2). Shing-Chung Wong and others also reported that thinner fibres can result in higher tensile strengths [43,44]. The tensile strength of the untreated PSI/PVA composite meshes as expected falls somewhere between the PSI and PVA meshes. No synergistic effect was observed verifying that no chemical bonding occurred between the two polymers only physical fibre to fibre contact. When comparing the treated samples PSI proved significantly weaker than the treated PVA meshes. Having no cross-links PSI meshes are more prone to tearing under the liquid as only physical bonds hold the fibres together unlike the PVA meshes [45]. In the same manner, treated PSI/PVA composite meshes also suffer from the absence of cross-linkage as they did not prove as strong as the treated PVA meshes. This result was expected as PSI was introduced into the system in order to degrade after a week and provide paths for the infiltrating cells around the mesh [46]. Comparing the PSI/PVA to the PVA meshes the decrease in tensile strength is not critical and there should not be difficulties during in vivo experiments as even implantation of hydrogels was possible [14,18,47,48]. Nevertheless, if required, several options for improvement of mechanical properties are available [49,50] (fibre alignment, additional crosslinkers, freezing treatment) and could be easily implemented if technical failures are observed during the In vivo experiments. Comparing the orientation of the samples to the collector, vertically aligned samples performed better as fibres can withstand more load when pulled along their own axis.

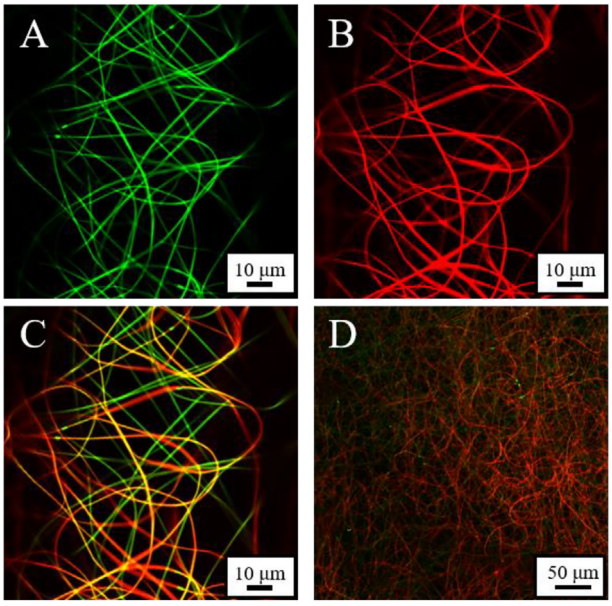

Fig. 6. TPEM micrographs of PSI/PVA meshes: green channel (A), red channel (B), both channels (C), both channels at lower magnifications (D).

Table 3
Wettability test results.

Mesh	Water angle
Dried PVA mesh	44.7°
Wet PVA mesh	66.4°
PSI mesh	Not measurable
PSI/PVA composite mesh	Not measurable

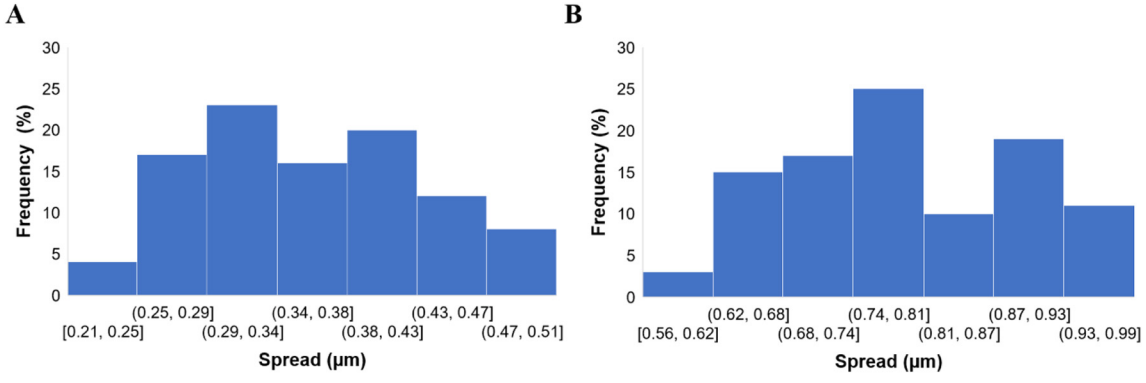

Fig. 5. Fibre size distribution of PSI/PVA meshes before (A) and after (B) treatment.

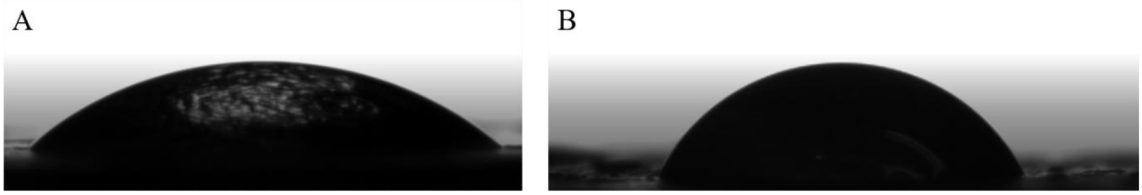

Fig. 7. Water angle of dry (A) and wet (B) PVA meshes.

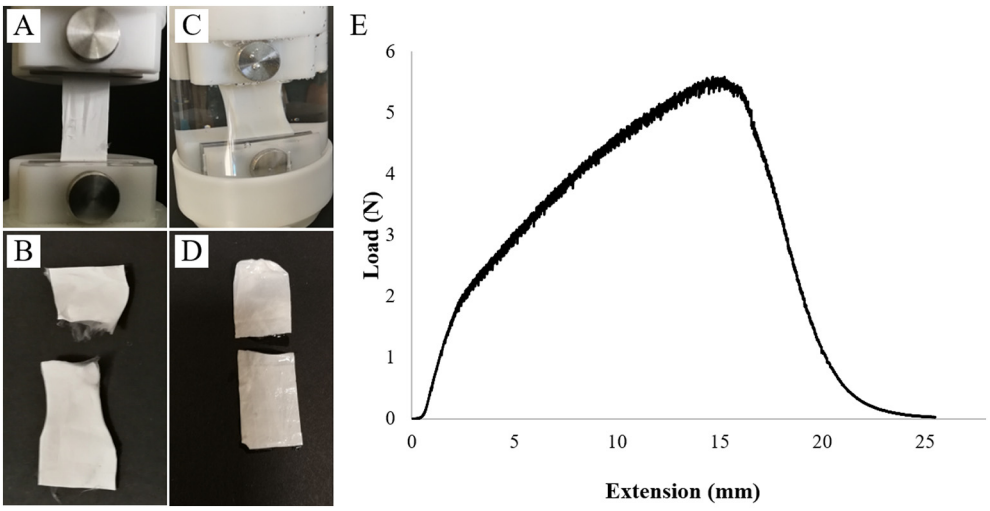

Fig. 8. Untreated PSI/PVA composite during(A) and after (B) measurement, treated PSI/PVA during (C) and after (D) measurement under buffer solution, typical stress-strain curve of the fabricated PSI/PVA meshes (E).

3.6. Cell viability results

For the cytotoxicity measurements, we used 2 different kinds of cell culture. The choice of the cell types was based on the different invasion capacity of the cultures. The MeWo is malignant melanoma, thus the cell proliferation and the invasion of the cells are more aggressive compared to the A2058. According to the results of the cell viability tests, no cytotoxic effects deriving from the meshes were observed (Fig. 9). Although the cell viability of the A2058 cells in the presence of the polymer meshes was lower compared to the control at 24 h, >2-fold increase in viability was detected by 48 h. In the case of MeWo cells, the viability in the treated groups was at a similar level as the control at 24 h, and increased values were measured in all the 4 groups by 48 h. Consequently, both cell types could not only survive but also proliferate in the presence of the PSI, PVA and PSI/PVA composite meshes.

Both cell types showed normal morphology throughout the whole experiment and no signs of cell death were revealed. A notable increase in cell number can be observed on the light microscopic images from 24 h to 48 h after the treatment with the meshes in each experimental group (see Supplementary Fig. 5). This finding also underlines that both cell types can survive and grow in the presence of the 3 types of polymer meshes. Similar positive results were previously reported by us and other groups as well [14,23,33,51,52].

Table 4
Results of the mechanical assessment.

Loading capacity (Nm^2/g)		
Mesh type	Horizontal alignment	Vertical alignment
PSI (in air)	0.235 ± 0.04	0.330 ± 0.07
PSI (in saline)	0.10 ± 0.007	0.095 ± 0.006
PVA (untreated, in air)	0.404 ± 0.04	0.553 ± 0.07
PVA (treated, in saline)	0.316 ± 0.06	1.064 ± 0.5
PSI/PVA composite (untreated, in air)	0.255 ± 0.02	0.325 ± 0.03
PSI/PVA composite (treated, in saline)	0.059 ± 0.01	0.177 ± 0.04

4. Conclusion

In the current manuscript, we presented the first attempt to combine electrospinning of PSI with PVA. The co-electrospinning proved successful and the concurrent presence of both polymers in the fabricated composite meshes was confirmed chemically via ATR-FTIR and visually via TPEM. The fibrous microstructure of the composite mesh was closely observed with SEM throughout the fabrication process and no damage was observed by either the mechanical or chemical treatment, a key parameter for tissue replacement. The mechanical parameters of the meshes were assessed by a uniaxial mechanical tester. Although the composite meshes did not perform as well as the pure PVA polymer meshes their performance should not provide difficulties during in vivo experiments. Cell viability studies were performed and no cytotoxic effect was detected in any of the meshes thus no contraindication for in vivo experiments on animals can be reported.

Declaration of competing interest

The authors confirm that this work is entirely original and no part of it has been published elsewhere, nor it is currently under consideration for publication elsewhere. We declare that there are no known conflicts of interest associated with this publication and there has been no financial support for this work that could have influenced its outcome.

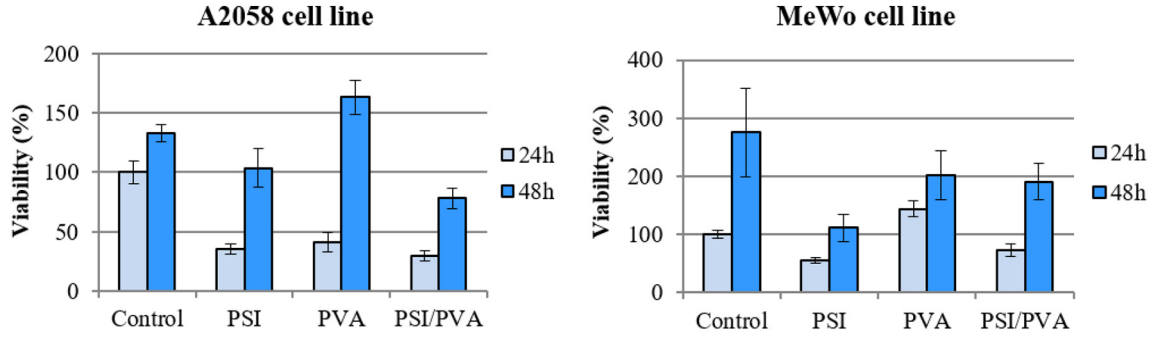

Fig. 9. Results of the cell viability studies of the 2 tumour cell lines. The viability values are normalized to the untreated control values measured 24 h after the treatment with the meshes. Data are given as arithmetic mean ± standard error of the mean.

Acknowledgements

This study was supported by the National Research, Development and Innovation Office – NKFIH FK 124147, the János Bolyai Research Scholarship of the Hungarian Academy of Sciences and by the ÚNKP-19-4-SE-04 New National Excellence Program of the Ministry for Innovation and Technology. The authors gratefully thank Gergő Gyulai for his assistance with the contact angle measurements and Ádám Péter for the assistance in the mechanical treatments.

Appendix. Supplementary data

Supplementary data to this article can be found online at https://doi.org/10.1016/j.molliq.2020.112895.

References

[1] B.A.C. Harley, I. V Yannas, Chapter 18 - in vivo synthesis of tissues and organs, in: R. Lanza, R. Langer, J. Vacanti (Eds.), Princ. Tissue Eng. (Fourth Ed.), Academic Press, Boston, 2014: pp. 325–355. doi:https://doi.org/10.1016/B978-0-12-398358-9.00018-5.

[2] K.L. Moffat, R.A. Neal, L.E. Freed, F. Guilak, Chapter 13 - engineering functional tissues: in vitro culture parameters, in: R. Lanza, R. Langer, J. Vacanti (Eds.), Princ. Tissue Eng, Fourth ed.Academic Press, Boston 2014, pp. 237–259, https://doi.org/10.1016/B978-0-12-398358-9.00013-6 , Fourth Edi.

[3] B. Basu, Biomaterials Science and Tissue Engineering: Principles and Methods, 1st edition Cambridge Univeristy Press, Cambridge, 2017.

[4] A. Khademhosseini, Y. Du, B. Rajalingam, J.P. Vacanti, R.S. Langer, Microscale technologies for tissue engineering, Adv. Tissue Eng. 103 (2008) 349–369, https://doi.org/10.1142/9781848161832_0017.

[5] Y. Liang, L. Li, R.A. Scott, K.L. Kiick, R. Road, Polymeric Biomaterials: Diverse Functions Enabled by Advances in Macromolecular Chemistry, 50, 2018 483–502, https://doi.org/10.1021/acs.macromol.6b02389.Polymeric.

[6] M.F. Maitz, Applications of synthetic polymers in clinical medicine, Biosurface and Biotribology 1 (2015) 161–176, https://doi.org/10.1016/j.bsbt.2015.08.002.

[7] M. Prakasam, J. Locs, K. Salma-Ancane, D. Loca, A. Largeteau, L. Berzina-Cimdina, Biodegradable materials and metallic implants—a review, J. Funct. Biomater. 8 (2017) 44, https://doi.org/10.3390/jfb8040044.

[8] K. Sharma, M.A. Mujawar, A. Kaushik, State-of-art functional biomaterials for tissue engineering, Front. Mater. 6 (2019) 1–10, https://doi.org/10.3389/fmats.2019.00172.

[9] D.F. Williams, Challenges with the development of biomaterials for sustainable tissue engineering, Front. Bioeng. Biotechnol. 7 (2019) 1–10, https://doi.org/10.3389/fbioe.2019.00127.

[10] P.A. Mouthuy, N. Zargar, O. Hakimi, E. Lostis, A. Carr, Fabrication of continuous electrospun filaments with potential for use as medical fibres, Biofabrication 7 (2015), 025006. https://doi.org/10.1088/1758-5090/7/2/025006.

[11] J. Xue, T. Wu, Y. Dai, Y. Xia, Electrospinning and electrospun nanofibers: methods, materials, and applications, Chem. Rev. 119 (2019) 5298–5415, https://doi.org/10.1021/acs.chemrev.8b00593.

[12] S. Nemati, S. jeong Kim, Y.M. Shin, H. Shin, Current progress in application of polymeric nanofibers to tissue engineering, Nano Converg 6 (2019) https://doi.org/10.1186/s40580-019-0209-y.

[13] M. Aslam, M.A. Kalyar, Z.A. Raza, Polyvinyl alcohol: a review of research status and use of polyvinyl alcohol based nanocomposites, Polym. Eng. Sci. 58 (2018) 2119–2132, https://doi.org/10.1002/pen.24855.

[14] K. Molnár, C. Voniatis, D. Fehér, A. Ferencz, L. Fónyad, L. Reiniger, M. Zrínyi, G. Wéber, A. Jedlovszky-Hajdú, Biocompatibility study of poly(vinyl alcohol)-based electrospun scaffold for hernia repair, Express Polym Lett 12 (2018) 676–687, https://doi.org/10.3144/expresspolymlett.2018.58.

[15] K. Jones, Chapter 9 - fibrotic response to biomaterials and all associated sequence of fibrosis, in: S.F. Badylak (Ed.), Host Response to Biomater, Academic Press, Oxford 2015, pp. 189–237, https://doi.org/10.1016/B978-0-12-800196-7.00009-8.

[16] J.M. Morais, F. Papadimitrakopoulos, D.J. Burgess, Biomaterials/tissue interactions: possible solutions to overcome foreign body response, AAPS J. 12 (2010) 188–196, https://doi.org/10.1208/s12248-010-9175-3.

[17] C. Lu, X. Wang, G. Wu, J. Wang, Y. Wang, H. Gao, J. Ma, An injectable and biodegradable hydrogel based on poly(alpha,beta-aspartic acid) derivatives for localized drug delivery, J. Biomed. Mater. Res. A 102 (2014) 628–638, https://doi.org/10.1002/jbm.a.34725.

[18] J.-C. Yeh, Y.-T. Hsu, C.-M. Su, M.-C. Wang, T.-H. Lee, S.-L. Lou, Preparation and characterization of biocompatible and thermoresponsive micelles based on poly(N-isopropylacrylamide-co-N,N-dimethylacrylamide) grafted on polysuccinimide for drug delivery, J. Biomater. Appl. 29 (2014) 442–453, https://doi.org/10.1177/0885328214533736.

[19] W. Cho, A New Biocompatible Coating for Bioanalytical Devices Based on PSI (Polysuccinimide), ETD Collect. Purdue Univ, 2020.

[20] E. Jalalvandi, A. Shavandi, Polysuccinimide and its derivatives: degradable and water soluble polymers (review), Eur. Polym. J. 109 (2018) 43–54, https://doi.org/10.1016/j.eurpolymj.2018.08.056.

[21] M.C. Gutiérrez, Z.Y. García-Carvajal, M. Jobbágy, F. Rubio, L. Yuste, F. Rojo, M.L. Ferrer, F. Del Monte, Poly(vinyl alcohol) scaffolds with tailored morphologies for drug delivery and controlled release, Adv. Funct. Mater. 17 (2007) 3505–3513, https://doi.org/10.1002/adfm.200700093.

[22] R.S. Sequeira, S.P. Miguel, C.S.D. Cabral, A.F. Moreira, P. Ferreira, I.J. Correia, Development of a poly(vinyl alcohol)/lysine electrospun membrane-based drug delivery system for improved skin regeneration, Int. J. Pharm. 570 (2019), 118640. https://doi.org/10.1016/j.ijpharm.2019.118640.

[23] D. Juriga, K. Nagy, A. Jedlovszky-Hajdú, K. Perczel-Kovách, Y.M. Chen, G. Varga, M. Zrínyi, Biodegradation and osteosarcoma cell cultivation on poly(aspartic acid) based hydrogels, ACS Appl. Mater. Interfaces 8 (2016) 23463–23476, https://doi.org/10.1021/acsami.6b06489.

[24] K. Molnar, A. Jedlovszky-Hajdu, M. Zrinyi, S. Jiang, S. Agarwal, Poly(amino acid)-based gel fibers with pH Responsivity by coaxial reactive electrospinning, Macromol. Rapid Commun. 38 (2017) 1–5, https://doi.org/10.1002/marc.201700147.

[25] M. Háková, L. Chocholoušová Havlíková, P. Solich, F. Švec, D. Šatínský, Electrospun nanofiber polymers as extraction phases in analytical chemistry – the advances of the last decade, TrAC - Trends Anal. Chem. 110 (2019) 81–96, https://doi.org/10.1016/j.trac.2018.10.030.

[26] M. Omidkhah, Facilitated transport of CO2 through EA-mediated poly(vinyl alcohol) membrane cross-linked by formaldehyde, J. Membr. Sci. Technol. 3 (2013) https://doi.org/10.4172/2155-9589.1000119.

[27] K. Molnar, D. Juriga, P.M. Nagy, K. Sinko, A. Jedlovszky-Hajdu, M. Zrinyi, Electrospun poly(aspartic acid) gel scaffolds for artificial extracellular matrix, Polym. Int. 63 (2014) 1608–1615, https://doi.org/10.1002/pi.4720.

[28] J. Vlasak, F. Rypaeek, J. Drobnik, V. Saudek, Properties And Reactivity of, vol. 64 (n.d.) 59–64.

[29] C. Niyangoda, T. Miti, L. Breydo, V. Uversky, M. Muschol, Carbonyl-based blue autofluorescence of proteins and amino acids, PLoS One 12 (2017) 1–15, https://doi.org/10.1371/journal.pone.0176983.

[30] X. Chen, W. Luo, H. Ma, Q. Peng, W.Z. Yuan, Y. Zhang, Prevalent intrinsic emission from nonaromatic amino acids and poly(amino acids), Sci. China Chem. 61 (2018) 351–359, https://doi.org/10.1007/s11426-017-9114-4.

[31] R. Rudra, V. Kumar, P.P. Kundu, Acid catalysed cross-linking of poly vinyl alcohol (PVA) by glutaraldehyde: effect of crosslink density on the characteristics of PVA membranes used in single chambered microbial fuel cells, RSC Adv. 5 (2015) 83436–83447, https://doi.org/10.1039/C5RA16068E.

[32] K. Kamemaru, S. Usui, Y. Hirashima, A. Suzuki, Irreversible swelling behavior and reversible hysteresis in chemically Crosslinked poly(vinyl alcohol) gels, Gels 4 (2018) 45, https://doi.org/10.3390/gels4020045.

[33] D. Juriga, E. Sipos, O. Hegedűs, G. Varga, M. Zrínyi, K.S. Nagy, A. Jedlovszky-Hajdú, Fully amino acid-based hydrogel as potential scaffold for cell culturing and drug delivery, Beilstein J. Nanotechnol. 10 (2019) 2579–2593, https://doi.org/10.3762/bjnano.10.249.

[34] C. Chai, Y. Xu, S. Shi, X. Zhao, Y. Wu, Y. Xu, L. Zhang, Functional polyaspartic acid derivatives as eco-friendly corrosion inhibitors for mild steel in 0.5 M H2SO4 solution, RSC Adv. 8 (2018) 24970–24981, https://doi.org/10.1039/c8ra03534b.
[35] H.S. Mansur, C.M. Sadahira, A.N. Souza, A.A.P. Mansur, FTIR spectroscopy characterization of poly (vinyl alcohol) hydrogel with different hydrolysis degree and chemically crosslinked with glutaraldehyde, Mater. Sci. Eng. C 28 (2008) 539–548, https://doi.org/10.1016/j.msec.2007.10.088.
[36] S. Chatterjee, S. Bhattacharjee, S.K. Maurya, V. Srinivasan, K. Khare, S. Khandekar, Surface wettability of an atomically heterogeneous system and the resulting intermolecular forces, Epl 118 (2017) https://doi.org/10.1209/0295-5075/118/68006.
[37] A.M. Matuska, P.S. McFetridge, The effect of terminal sterilization on structural and biophysical properties of a decellularized collagen-based scaffold; implications for stem cell adhesion, J. Biomed. Mater. Res. - Part B Appl. Biomater. 103 (2015) 397–406, https://doi.org/10.1002/jbm.b.33213.
[38] H. Jeon, H. Lee, G. Kim, A surface-modified poly(ε-caprolactone) scaffold comprising variable nanosized surface-roughness using a plasma treatment, Tissue Eng. - Part C Methods. 20 (2014) 951–963, https://doi.org/10.1089/ten.tec.2013.0701.
[39] Surface Design: Applications in Bioscience and Nanotechnology. , John Wiley & Sons, Ltd, 2009 I–XXI, https://doi.org/10.1002/9783527628599.fmatter.
[40] Y. Fang, L. Xu, M. Wang, High-throughput preparation of silk fibroin nanofibers by modified bubble-electrospinning, Nanomaterials 8 (2018) 1–20, https://doi.org/10.3390/nano8070471.
[41] A.L. Butcher, C.T. Koh, M.L. Oyen, Systematic mechanical evaluation of electrospun gelatin meshes, J. Mech. Behav. Biomed. Mater. 69 (2017) 412–419, https://doi.org/10.1016/j.jmbbm.2017.02.007.
[42] L. De Siqueira, N. Ribeiro, M.B.A. Paredes, L. Grenho, C. Cunha-reis, E.S. Trich, M.H. Fernandes, S.R. Sousa, Influence of PLLA/PCL/HA Scaffold Fiber Orientation on Mechanical Properties and Osteoblast Behavior, 2019.
[43] P. Kumar, R. Vasita, Understanding the relation between structural and mechanical properties of electrospun fiber mesh through uniaxial tensile testing, J. Appl. Polym. Sci. 134 (2017) 1–11, https://doi.org/10.1002/app.45012.
[44] S.C. Wong, A. Baji, S. Leng, Effect of fiber diameter on tensile properties of electrospun poly(ε-caprolactone), Polymer (Guildf) 49 (2008) 4713–4722, https://doi.org/10.1016/j.polymer.2008.08.022.
[45] A. Pinheiro, A. Cooley, J. Liao, R. Prabhu, S. Elder, Comparison of natural crosslinking agents for the stabilization of xenogenic articular cartilage, J. Orthop. Res. 34 (2016) 1037–1046, https://doi.org/10.1002/jor.23121.
[46] A.P. Mathew, K. Oksman, M. Sain, Mechanical properties of biodegradable composites from poly lactic acid (PLA) and microcrystalline cellulose (MCC), J. Appl. Polym. Sci. 97 (2005) 2014–2025, https://doi.org/10.1002/app.21779.
[47] B.W. Renz, K. Leitner, E. Odermatt, D.L. Worthley, M.K. Angele, K.W. Jauch, R.A. Lang, PVA gel as a potential adhesion barrier: a safety study in a large animal model of intestinal surgery, Langenbeck's Arch. Surg. 399 (2014) 349–357, https://doi.org/10.1007/s00423-013-1159-1.
[48] Y. Qu, B.Y. Chu, J.R. Peng, J.F. Liao, T.T. Qi, K. Shi, X.N. Zhang, Y.Q. Wei, Z.Y. Qian, A biodegradable thermo-responsive hybrid hydrogel: therapeutic applications in preventing the post-operative recurrence of breast cancer, NPG Asia Mater 7 (2015) e207–e210, https://doi.org/10.1038/am.2015.83.
[49] T. Stylianopoulos, C.A. Bashur, A.S. Goldstein, S.A. Guelcher, V.H. Barocas, Computational predictions of the tensile properties of electrospun fibre meshes: effect of fibre diameter and fibre orientation, J. Mech. Behav. Biomed. Mater. 1 (2008) 326–335, https://doi.org/10.1016/j.jmbbm.2008.01.003.
[50] M. Cho, M.A. Karaaslan, S. Renneckar, F. Ko, Enhancement of the mechanical properties of electrospun lignin-based nanofibers by heat treatment, J. Mater. Sci. 52 (2017) 9602–9614, https://doi.org/10.1007/s10853-017-1160-0.
[51] C.Y. Huang, K.H. Hu, Z.H. Wei, Comparison of cell behavior on pva/pva-gelatin electrospun nanofibers with random and aligned configuration, Sci. Rep. 6 (2016) 1–8, https://doi.org/10.1038/srep37960.
[52] O. Hegedus, D. Juriga, E. Sipos, C. Voniatis, Á. Juhász, A. Idrissi, M. Zrínyi, G. Varga, A. Jedlovszky-Hajdú, K.S. Nagy, Free thiol groups on poly(aspartamide) based hydrogels facilitate tooth-derived progenitor cell proliferation and differentiation, PLoS One 14 (2019) 1–20, https://doi.org/10.1371/journal.pone.0226363.